2007

A 28-ka history of sea surface temperature, primary productivity and planktonic community variability in the western Arabian Sea

A Pourmand

F Marcantonio

TS Bianchi

EA Canuel
Virginia Institute of Marine Science

EJ Waterson
Virginia Institute of Marine Science

A 28-ka history of sea surface temperature, primary productivity and planktonic community variability in the western Arabian Sea

Ali Pourmand,[1,2] Franco Marcantonio,[1,3] Thomas S. Bianchi,[1,4] Elizabeth A. Canuel,[5] and Elizabeth J. Waterson[5]

[1] Uranium series radionuclides and organic biomarkers, which represent major groups of planktonic organisms, were measured in western Arabian Sea sediments that span the past 28 ka. Variability in the past strength of the southwest and northeast monsoons and its influence on primary productivity, sea surface temperature (SST), and planktonic community structure were investigated. The average alkenone-derived SST for the last glacial period was ~3°C lower than that measured for the Holocene. Prior to the deglacial, the lowest SSTs coincide with the highest measured fluxes of organic biomarkers, which represent primarily a planktonic suite of diatoms, coccolithophorids, dinoflagellates, and zooplankton. We propose that intensification of winter northeast monsoon winds during the last glacial period resulted in deep convective mixing, cold SSTs and enhanced primary productivity. In contrast, postdeglacial (<17 ka) SSTs are warmer during times in which biomarker fluxes are high. Associated with this transition is a planktonic community structure change, in which the ratio of the average cumulative flux of diatom biomarkers to the cumulative flux of coccolithophorid biomarkers is twice as high during the deglacial and Holocene than the average ratio during the last glacial period. We suggest that this temporal transition represents a shift from a winter northeast monsoon-dominated (pre-17 ka) to a summer southwest monsoon-dominated (post-17 ka) wind system.

Citation: Pourmand, A., F. Marcantonio, T. S. Bianchi, E. A. Canuel, and E. J. Waterson (2007), A 28-ka history of sea surface temperature, primary productivity and planktonic community variability in the western Arabian Sea, *Paleoceanography*, *22*, PA4208, doi:10.1029/2007PA001502.

1. Introduction

[2] Seasonal reversal in the pattern of atmospheric circulation across the northern Indian Ocean and central Asia is a major feature of the Earth's climate. During summer, the southwest monsoon (SWM) is responsible for most of annual precipitation across a large area from eastern Africa to the Indian subcontinent. As the Tibetan Plateau is heated, a gradient of temperature and pressure is formed over the northern Indian Ocean and central Asia, which initiates an expansive atmospheric flow from south of the equator [*Clemens et al.*, 1991]. This flow is accompanied by the low-level Findlater Jet [*Findlater*, 1974] that blows parallel to the coast of the Arabian Peninsula and induces a complex pattern of Ekman transport away from coastal regions in the western Arabian Sea. The filaments and eddies of cold nutrient-rich water that form as a result of Ekman transport

stimulate high levels of primary production in the western Arabian Sea, and parts of the northeastern Arabian Sea along the Pakistani margin [e.g., *Brock and McClain*, 1992; *Honjo et al.*, 1999; *Nair et al.*, 1989]. During the modern-day SWM, sea surface temperatures (SSTs) on the Oman margin reach values as low as 23–24°C within the upwelling region [*Dahl and Oppo*, 2006] and increase from west to east with distance from the coast. The SWM-induced upwelling is responsible for 67% of total new primary production in the world oceans [*Chavez and Toggweiler*, 1995] and hence plays an important role in the global carbon cycle. Indeed, on glacial-interglacial timescales, the extent to which the Arabian Sea behaves as a sink for CO_2 may exert control on the efficiency of the global biological pump [*Rixen et al.*, 2005], which, in turn, may influence global climate via feedback mechanisms [*Hales et al.*, 2005].

[3] The pattern of summer atmospheric circulation is reversed as temperature and pressure gradients between the Indian Ocean and the Tibetan Plateau change direction during the winter. Consequently, the northeast monsoon (NEM) dominates over most of the northern Indian Ocean during the winter season. The NEM also induces relatively high levels of primary productivity by lowering the SST and thereby increasing the depth of the mixed layer through convective mixing [*Haake et al.*, 1993; *Wakeham et al.*, 2002]. As a result of this mixing, nutrients that are otherwise trapped below the thermocline are mixed into the euphotic zone and become available to primary producers.

---

[1]Department of Earth and Environmental Sciences, Tulane University, New Orleans, Louisiana, USA.

[2]Now at Department of Geophysical Sciences, University of Chicago, Chicago, Illinois, USA.

[3]Now at Department of Geology and Geophysics, Texas A&M University, College Station, Texas, USA.

[4]Now at Department of Oceanography, Texas A&M University, College Station, Texas, USA.

[5]Virginia Institute of Marine Science, College of William and Mary, Gloucester Point, Virginia, USA.
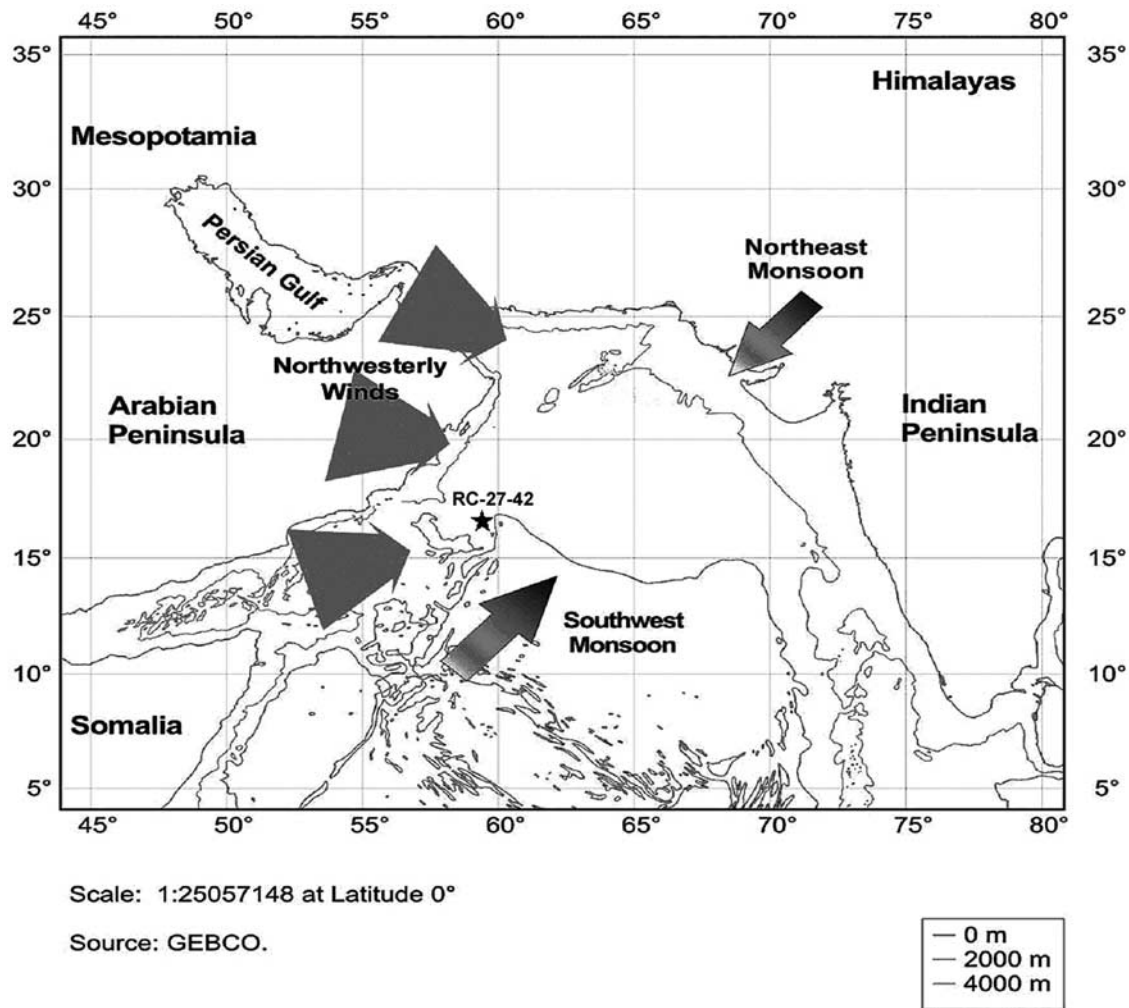
Figure 1. Position of core RC-27-42 in the western Arabian Sea in relation to major wind systems indicated by the arrows.

Sea surface temperatures in the modern-day northeastern Arabian Sea undergo a cooling of up to 3–4°C during the NEM [*Dahl and Oppo*, 2006; *Emeis et al.*, 1995].

[4] The strength of the SWM relative to the NEM has been variable during the last glacial-interglacial cycles as a consequence of three interrelated mechanisms: (1) changes in seasonal solar insolation and sensible heat, (2) variability in availability and transport of latent heat from south of the equator, and (3) changes in glacial boundary conditions (i.e., extent of snow coverage across central Asia and the Tibetan Plateau and subsequent increase in continental albedo [*Naidu*, 1998]). In order to shed light on the dynamics of SWM and NEM and their connection to global climate change over orbital and suborbital timescales during the late Pleistocene and Holocene, numerous inorganic and organic geochemical proxies have been measured in sediments from the northern Indian Ocean [e.g., *Altabet et al.*, 2002; *Clemens and Prell*, 1990; *Higginson et al.*, 2004; *Marcantonio et al.*, 2001; *Pourmand et al.*, 2004; *Rogalla and Andruleit*, 2005; *Rostek et al.*, 1997; *Schulte et al.*, 1999; *Schulz et al.*, 1998; *Sirocko et al.*, 2000]. We know

that relatively higher levels of primary production occur during the modern-day SWM in the western and northeastern Arabian Sea compared with production during the NEM [*Honjo et al.*, 1999; *Wakeham et al.*, 2002], However, the sediment record suggests a more complex relationship between summer and winter monsoon intensity [*Budziak et al.*, 2000; *Dahl and Oppo*, 2006; *Reichart et al.*, 1998]. While most studies of sediments in the western Arabian Sea report low primary production during the last glacial period when the SWM was relatively weak, there is also some evidence that indicates the opposite trend (i.e., equal or higher amounts of primary production during the last glacial maximum (LGM) due to an intensified winter NEM) [*Banakar et al.*, 2005; *Naidu and Malmgren*, 2005; *Tamburini et al.*, 2003].

[5] In this study we measured several organic and inorganic climate proxies in sediments from core RC-27-42 in the western Arabian Sea in order to determine the extent to which changes in SW and NE monsoon intensities control past variations in primary production, sea surface temperature, eolian fluxes and planktonic community structure. The

organic biomarker proxy data allowed us to estimate down-core variability in (1) SSTs and (2) ^{230}Th-normalized fluxes of three dominant phytoplankton groups (i.e., diatoms, coccoli-thophorids, dinoflagellates) and zooplankton. These estimates also made it possible to examine the relationship between regional/global climate change and past variations in Arabian Sea SSTs and planktonic community structure.

2. Analytical Methodology

2.1. Age Model

[6] Core RC-27-42 (obtained from Lamont-Doherty Earth Observatory Core Repository) was retrieved from the western Arabian Sea (16.5°N, 59.8°E; 2040 m water depth; Figure 1) ∼350 km from the Oman continental margin. The location of this core places it within the zone of intense upwelling induced by today's summer SWM [e.g., *Dahl and Oppo*, 2006]. A total of 150 stable oxygen isotopic ratios (δ^{18}O) were measured in the tests of the foraminifera *Globigerinoides ruber* in order to establish an age model for this core. The sediment samples were washed through a series of wire mesh sieves to isolate the tests between 300 and 450 μm. Oxygen isotope ratios were measured at the Georgia Institute of Technology in the laboratory of J. Lynch-Stieglitz. The oxygen isotope results are expressed in per mil (‰) relative to standard mean ocean water (SMOW). The overall precision of each analysis is better than 0.05‰. We used the AnalySeries V.2.0 software [*Paillard et al.*, 1996] to tune our oxygen isotope record to the SPECMAP marine oxygen isotope record [*Martinson et al.*, 1987]. Six samples were also selected for radiocarbon analysis in order to refine our preliminary oxygen isotope age model. Two to four mg of *Globigerinoides sacculifer* tests (>300 μm) were hand-selected for radiocarbon accelerator mass spectrometry dating at the Woods Hole's NOSAMS facility. Radiocarbon ages were corrected for the average reservoir uncertainty age (ΔR) of 208 ± 50 a using data from 16 sites in the Arabian Sea [*Bhushan et al.*, 1994; *Dutta et al.*, 2001; *Southon et al.*, 2002]. The ages were then calibrated to calendar years before present (1950) using the Calib 5.0 software [*Stuiver and Reimer*, 1993] and the University of Cologne radiocarbon calibration (B. Weninger et al., CalPal-2007, Cologne Radiocarbon Calibration and Palaeoclimate Research Package, http://www.calpal.de). The calibrated calendar ages range from 7627 to 26,595 a B.P. (Figure 2a).

2.2. Uranium Series Radionuclides

2.2.1. Radionuclide Analyses

[7] Approximately 0.4 to 0.6 g of dried and homogenized sediments were spiked with solutions containing known concentrations of ^{236}U and ^{229}Th. The samples were digested with concentrated HNO$_3$, HF, HCl and HClO$_4$ and converted to a solution of 3M HNO$_3$-1M Al(NO$_3$)$_3$ after complete dissolution. Uranium and thorium were isolated using prepacked Eichrom U/TEVA and TEVA cartridges under vacuum conditions. Uranium and thorium concentrations and isotopic ratios were analyzed by isotope dilution using an axiom inductively coupled plasma

mass spectrometer (ICP-MS) at the Lamont-Doherty Earth Observatory.

[8] Abundance sensitivity corrections, estimated using half-mass counting intensities, were applied to the lower-abundance ^{234}U, ^{235}U, ^{236}U, ^{229}Th, and ^{230}Th masses. The natural atomic ^{238}U/^{235}U ratio of 137.88 was used to monitor and correct for mass fractionation, which ranged from 1 to 5‰ per atomic mass unit (amu). Excess ^{230}Th (hereafter xs-^{230}Th) activities, the unsupported scavenged fraction of ^{230}Th, were calculated as follows:

$$
\begin{aligned}
\text{xs-}^{230}\text{Th} = \text{Total}\left(^{230}\text{Th}\right)_{\text{sample}} \\
- \left[\left(^{238}\text{U}/^{232}\text{Th}\right)_{\text{detrital}} * \text{Total}\left(^{232}\text{Th}\right)_{\text{sample}}\right] \\
- \left\{\left[\left(^{238}\text{U}\right)_{\text{sample}}\right.\right. \\
\left.- \left(^{238}\text{U}/^{232}\text{Th}\right)_{\text{detrital}} * \text{Total}\left(^{232}\text{Th}\right)_{\text{sample}}\right] \\
\left. * \ ^{230}\text{Th}_{\text{in-growth}}\right\}
\end{aligned}
\tag{1}
$$

The second term (in brackets) on the right-hand side of the equation accounts for the ^{230}Th activity supported by the uranium activity in material from lithogenic sources, and the third term (in braces) represents the ^{230}Th that accumulates from the time of deposition due to the decay of authigenic U. In order to calculate both of these corrections, we use a detrital ^{238}U/^{232}Th activity ratio of 0.62 [see *Pourmand et al.*, 2005]. External reproducibility is less than 5% for U and Th concentrations.

2.2.2. Excess ^{230}Th-Normalized Mass Accumulation Rates

[9] The flux of ^{230}Th to sediments in 70% of the world's oceans is within 30% of that expected from vertical production [*Francois et al.*, 2004; *Henderson et al.*, 1999]. This is the basis for using measured ^{230}Th in sediments as a constant flux proxy to calculate sediment mass accumulation rates. Briefly, ^{230}Th (half-life of 75.2 ka) is produced in the water column through α decay of ^{234}U. As ^{230}Th has a short residence time in the water column (∼20 a [*Henderson and Anderson*, 2003]), it is scavenged by particles nearly as quickly as it is produced. Because the rate of ^{230}Th removal from the water column into the underlying sediments is approximately equal to its rate of production, mass accumulation rates (MARs) can be estimated as follows:

$$
\text{MAR} = \left[\beta_{\text{Th}} * Z\right]/\left(\text{xs-}^{230}\text{Th}_{\text{o}}\right)
\tag{2}
$$

where Z represents the water depth in m, and β_{Th} represents the rate of production of ^{230}Th in the water column and is equal to 2.63×10^{-3} disintegrations per minute (dpm) cm^{-3} ka^{-1}. (xs-^{230}Th$_{\text{o}}$) is the activity of ^{230}Th that is in excess of (i.e., not supported by) the activity of ^{234}U in the sediment at the time of deposition. One of the major advantages of xs-^{230}Th-derived MARs is that such estimates are insensitive to sediment redistribution processes by bottom currents [e.g., *Marcantonio et al.*, 2001]. A review
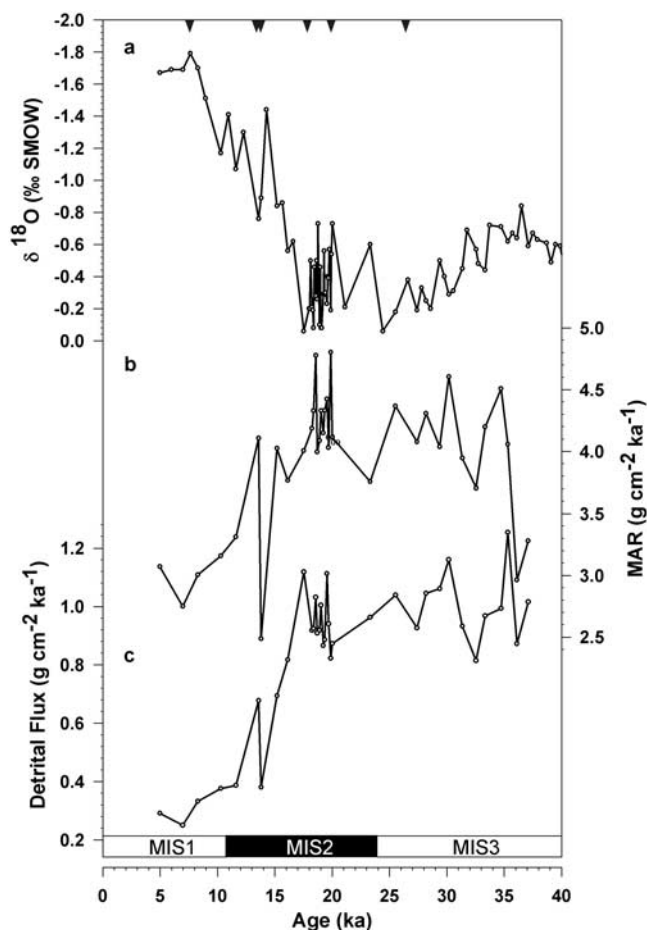
Figure 2. (a) Oxygen isotope ratios for hand-picked specimens of *G. ruber* in core RC-27-42. The age model was obtained by tuning the record with SPECMAP [*Paillard et al.*, 1996] and refined using six calibrated radiocarbon dates (triangles). (b) Excess ^{230}Th-derived mass accumulation rates from RC-27-42 for the past 37 ka. (c) Excess ^{230}Th-derived detrital (eolian) mass accumulation rates from RC-27-42 for the past 37 ka. Mass accumulation rates (MARs) of eolian material remain high during the entire glacial period and drop precipitously beginning at about 17 ka. Marine isotopic stages (MIS) 1–3 are shown in inset at the bottom of the graph.

of xs-^{230}Th constant flux profiling technique and applications is given by *Francois et al.* [2004].

2.3. Organic Geochemistry

2.3.1. Extraction of Lipids

[10] Lipid compounds were extracted from oven-dried (at 40°C) and homogenized sediment samples (1.5–3.5 g) with accelerated solvent extraction (ASE) using methylene chloride and methanol (CH$_2$Cl$_2$:CH$_3$OH, 2:1, v:v). Organic and aqueous fractions were partitioned following the addition of CH$_3$OH and a 20% NaCl solution. The organic fraction was then dried at the presence of Na$_2$SO$_4$ overnight and concentrated by turbo evaporation. The lipid extract was saponified at 110°C with 1N KOH in 80% aqueous CH$_3$OH [*Canuel and Martens*, 1993]. The neutral lipids were extracted using hexane and sterol compounds were converted to their (trimethylsilyl) ether derivatives (TMS) at 80°C using 250 μL of BSTFA (bis(trimethylsilyl)-trifluoroacetamide) and 500 μL of acetonitrile.

2.3.2. Gas Chromatography and Mass Spectrometry

[11] All organic biomarker compounds were analyzed on a Hewlett-Packard 5890 Series II gas chromatograph equipped with a flame ionization detector (GC-FID) using a cool on-column injector and helium as the carrier gas. The 5α(H)-cholestane was added as an internal standard to each sample prior to GC-FID analysis for compound quantification. Compound identifications were verified using a Hewlett-Packard 6890 Gas Chromatograph with a mass selective detector (GC-MSD). Both GC-MSD and GC-FID were equipped with a J&W Scientific DB-5 60 m × 0.32 mm i.d. column coated with 0.25 μm of a nonpolar phase. A dual temperature ramp was implemented with an initial temperature program of 80°C to 120°C at 20°C per minute, followed by 120°C to 320°C at 10°C per minute. The temperature was held at 320°C for 20 min. The overall analytical error for biomarker analyses was between 10 and 15%.

3. Results

3.1. Inorganic Geochemical Proxies

3.1.1. The ^{230}Th-Normalized MARs

[12] The average flux of ^{230}Th to the sediments over the last 37 ka can be calculated by multiplying the average age-model-derived linear sedimentation rate (5.44 cm ka^{-1}), by the average ^{230}Th activity (1.40 dpm g^{-1}; Table 1) and the average dry bulk density (0.68 g cm^{-3}; average value from five nearby cores in the western Arabian Sea [*Sirocko*, 1991]). We determine an average ^{230}Th flux of 5.18 dpm cm^{-2} ka^{-1} that is within 30% of that expected from production of ^{230}Th from ^{234}U decay in the water column (5.36 dpm cm^{-2} ka^{-1}). A ^{230}Th flux to production ratio of near unity indicates that, on average, little to no lateral advection of sediment has occurred. It is expected therefore that the majority of sediment at this site was supplied by vertical rain through the water column. We reached the same conclusion in our study of sediments spanning the last 110 ka in core 93 KL from the northeastern Arabian Sea [*Pourmand et al.*, 2004].

[13] Excess ^{230}Th-derived sediment MARs in core RC-27-42 was determined over the last 38 ka (Table 1 and Figure 2b) with average glacial MARs of about 35% greater than those measured for the Holocene sediments.

3.1.2. Glacial-Holocene Variability in Detrital (Eolian) Fluxes

[14] The location of core RC-27-42 in the western Arabian Sea places it within the zone of high dust input supplied by northwesterly, SWM, and NEM winds (Figure 1) [*Sirocko and Lange*, 1991]. Riverine fluxes from the Oman margin are insignificant, making eolian input the main contributor of detrital material to the western Arabian Sea [e.g., *Sirocko et al.*, 2000].

Table 1. Sample Depths, Age Model, and U-Th Data[a]

Sample Depth, cm	Age Model, ka	xs-^{230}Th$_o$, dpm/g	^{232}Th, ppm	U Authigenic, ppm
15	5.0	1.75	1.02	3.10
21	7.0	1.95	0.97	3.66
23	**7.6**	-	-	-
25	8.3	1.79	1.18	3.71
31	10.3	1.70	1.28	3.90
35	11.6	1.62	1.25	3.97
41	**13.6**	1.31	1.77	3.36
45	**13.8**	2.16	1.64	3.80
51	15.2	1.33	1.85	3.23
55	16.1	1.43	2.32	3.26
61	17.5	1.34	2.99	2.81
63	**18.0**	-	-	-
71	18.2	1.28	2.35	3.84
75	18.4	1.24	2.28	4.01
81	18.6	1.12	2.31	3.71
85	18.7	1.34	2.43	3.88
91	18.9	1.31	2.40	4.11
95	19.0	1.24	2.48	4.14
101	19.2	1.29	2.23	4.00
105	19.4	1.24	2.19	4.06
111	19.5	1.21	2.69	2.95
115	19.7	1.33	2.50	2.62
121	19.9	1.12	1.83	2.50
125	**20.0**	1.30	2.27	2.81
131	23.3	1.43	2.74	4.36
135	25.5	1.23	2.55	4.20
137	**26.6**	-	-	-
141	27.4	1.32	2.43	3.27
145	28.2	1.25	2.60	3.16
151	29.4	1.33	2.81	2.71
155	30.2	1.16	2.70	2.50
161	31.4	1.36	2.53	3.13
167	32.5	1.45	2.35	3.44
171	33.3	1.28	2.47	3.00
178	34.7	1.19	2.36	2.94
181	35.3	1.32	3.31	3.04
185	36.1	1.81	3.15	3.85
190	37.1	1.64	3.31	2.49

[a]Bold data represent radiocarbon calendar ages.

[15] The ^{230}Th-derived MARs and ^{232}Th concentrations (Table 1) were used to calculate the flux of ^{232}Th, which is a proxy for eolian input [e.g., *McGee et al.*, 2007]. Assuming that the average concentration of ^{232}Th in eolian material (10.7 ppm [*Taylor and McLennan*, 1985]) has remained constant throughout our record, we have converted ^{232}Th

fluxes to eolian fluxes (Figure 2c). It is evident from Figure 2c that the average flux of eolian material during the Holocene (0.33 g cm^{-2} ka^{-1}) is almost 3 times lower than the glacial average of 0.93 g cm^{-2} ka^{-1}.

3.2. Organic Biomarkers

[16] A total of nine organic compounds including C$_{27}$−C$_{29}$ sterols and C$_{37}$−C$_{39}$ methyl ketones (alkenones) were quantified in this study (Table 2). In order to minimize the influence of dilution by terrigenous input, we have converted concentrations of biomarkers to accumulation rates using ^{230}Th-derived MARs (biomarker flux = biomarker concentration * ^{230}Th-derived MAR).

[17] Dehydrocholesterol, brassicasterol, 24-methylene cholesterol and 24-ethylcholest-5-en-3β-ol are biomarkers that primarily represent diatoms [e.g., *Dahl et al.*, 2004; *Werne et al.*, 2000]. 24-methylene cholesterol has been proposed by *Wakeham et al.* [2002] as the best indicator for diatoms in the modern-day Arabian Sea. While in this study we associate 24-ethylcholest-5-en-3β-ol with diatoms, this biomarker can also be produced by higher plants (C$_3$ and C$_4$) and some species of microalgae and cynaobacteria. Indeed, terrigenous source(s) for 24-ethylcholest-5-en-3β-ol (e.g., wind-blown plant material originating from Mesopotamia and the Arabian Peninsula) cannot be completely ruled out. There is, however, no discernible relationship between the fluxes of detrital material (Figure 2c) and 24-ethylcholest-5-en-3β-ol (Figure 3d) over the last 30 ka (r^2 at 95% confidence = 0.05), as would be expected were 24-ethylcholest-5-en-3β-ol to have an eolian origin. Furthermore, the changes in the fluxes of 24-ethylcholest-5-en-3β-ol covary with other diatom biomarkers (Figure 3), suggesting diatoms as a viable source for this compound.

[18] The most prominent features in Figure 3 are that (1) all diatom biomarker fluxes (Table 3) follow the same pattern of variability (Figures 3a−3d), and (2) there does not seem to be a considerable change in the amplitude of the high-frequency flux cycles through time, except for the brassicasterol, which shows a more pronounced decrease in the amplitude of flux cycles later in the record (Figure 3b).

[19] We use 23,24-dimethyl-5α(H)-cholest-22-en-3β-ol and 4α,23,24-trimethyl-5α(H)-cholest-22-en-3β-ol (dinosterol) as biomarker proxies for dinoflagellates (Figure 4). The fluxes of dinoflagellate biomarkers (Table 3) display a pattern that is synchronous with that found for the fluxes of diatom biomarkers. In contrast to the pattern of variability

Table 2. List of Organic Compounds Quantified for This Study and Their Commonly Used Names and Possible Origin

Organic Compounds	Common Name	Source Organisms
Cholesta-5,22-dien-3b-ol	dehydrocholesterol	diatoms,[a] red algae
24-methylcholesta-5,22(E)-dien-3b-ol	brassicasterol	diatoms,[a] coccolithophores
24-methylcholesta-5,24(28)-dien-3b-ol	24-methylene cholesterol	diatoms,[a] brown algae
24-ethylcholest-5-en-3b-ol	-	diatoms,[a] C3, C4 plants
23,24-dimethyl-5a(H)-cholest-22-en-3b-ol	-	dinoflagellate
4a,23,24-trimethyl-5a (H)-cholest-22-en-3b-ol	dinosterol	dinoflagellate
Heptatriaconta-15E,22(E)-trien-2one	C$_{37:3}$ alkenone	coccolithophorids
Heptatriaconta-15E,22(E)-dien-2one	C$_{37:2}$ alkenone	coccolithophorids
Cholest-5-en-3b-ol	Cholesterol	zooplankton,[a] Phytoplankton

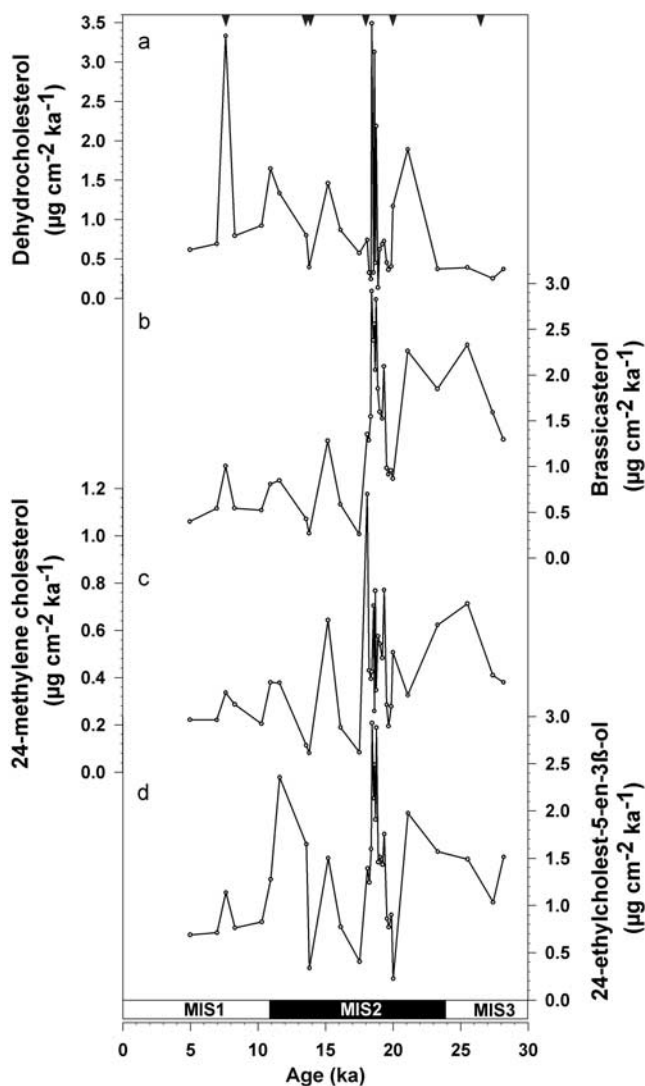[a]Main group of plankton associated with the compound in this study.

Figure 3. The ^{230}Th-normalized mass accumulation rates of (a) dehydrocholesterol, (b) brassicasterol, (c) 24-methylene cholesterol, and (d) 24-ethylcholest-5-en-3β-ol over the last 28 ka. The calibrated radiocarbon dates (triangles at top) and marine isotopic stages (MIS) 1−3 (inset at bottom) are also shown.

observed in the diatom biomarkers, however, the amplitude of the high-frequency flux cycles of dinoflagellate biomarkers decreases from 28 to 5 ka (Figures 4a and 4b).

[20] Coccolithophorids (e.g., *Emiliania huxleyi* and *Gephyrocapsa oceanica*) of the class Haptophytes are the main producers of diunsaturated and triunsaturated methyl ketones ($C_{37:2}$ and $C_{37:3}$, respectively) [*Conte et al.*, 1994; *Rostek et al.*, 1997]. Coccolithophorids are also important contributors to primary production in the Arabian Sea today [e.g., *Honjo et al.*, 1999]. Total C_{37} alkenone concentrations or fluxes have been widely employed as a qualitative proxy for paleoproduction and monsoon intensity [*Budziak et al.*, 2000; *Schubert et al.*, 1998]. Lowest and highest fluxes of alkenones (cumulative fluxes of $C_{37:2}$ and $C_{37:3}$) vary

between 0.79 and 8.82 μg cm^{-2} ka^{-1}, respectively (Table 3 and Figure 4c). The pattern of periodic variability observed in the sterol biomarker fluxes is not as strong in the alkenone fluxes.

[21] Cholesterol, the dominant sterol in crustaceans such as zooplankton, is also present in fecal pellets and is associated with zooplankton grazing [*Wakeham et al.*, 2002, and references therein]. Although cholesterol is typically the most abundant sterol in zooplankton, it can derive from additional sources, including phytoplankton (e.g., at trace levels in some microalgae [*Volkman*, 1986]). The fluxes of cholesterol range between 0.23 and 2.6 μg cm^{-2} ka^{-1} (Figure 4d). The pattern of variability for cholesterol is similar to that for the other sterol biomarker fluxes over the entire record.

[22] Prior to 17 ka (the beginning of the last deglacial; δ^{18}O, Figure 5a), the average cumulative biomarker flux (CBF) is higher (13.9 μg cm^{-2} ka^{-1}) than after 17 ka (6.5 μg cm^{-2} ka^{-1}). In addition, the average CBFs show the same pattern of variability that is displayed by each individual organic biomarker flux.

4. Discussion

4.1. $U_{37}^{K'}$ Sea Surface Temperature Estimates

[23] $C_{37}-C_{39}$ alkenones are produced by a few phytoplankton species of class Prymnesiophyceae and provide information about sea surface temperature variability in the past. Laboratory culturing experiments and measurements from marine sediments have shown that the relative composition of the $C_{37:2}$, $C_{37:3}$, and $C_{37:4}$ (diunsaturated, triunsaturated, and tetraunsaturated methyl and ethyl ketones) appears to be closely correlated with the temperature of the water in which coccolithophorids grow [*Brassell et al.*, 1986; *Prahl and Wakeham*, 1987; *Rostek et al.*, 1997]. Hence estimates of past SSTs can be made by measuring the unsaturation ratio of C_{37} alkenones in sediments. Alkenones appear to be resistant to food web processes [e.g., *Rowland and Volkman*, 1982], sedimentary degradation during diagenesis [*Prahl et al.*, 2003], and even exposure to air for long periods (T. Eglinton, personal communication, 2005). It has also been shown that the unsaturation ratio of C_{37} alkenones does not appear to be affected by changes in community structure of haptophyte algae during the Late Quaternary [*Herbert et al.*, 1998]. The $C_{37:4}$ alkenone is absent in our sediments since it is mainly produced by organisms that dwell in the colder waters of higher latitudes. Therefore the modified alkenone unsaturation index can be expressed as

$$U_{37}^{K'} = [C_{37:2}]/[C_{37:2} + C_{37:3}] \qquad (3)$$

[24] The relationship between $U_{37}^{K'}$ and SST is established empirically between cultures of *G. oceanica* and *E. huxleyi* and controlled growth temperature [*Prahl et al.*, 1988]. At our core site, average $U_{37}^{K'}$ values range between 0.80 and 0.91 over the past 30 ka with the lowest values occurring between 18 and 19 ka (Figure 5d). In order to convert $U_{37}^{K'}$ to SST, we employed the empirical relationship established by *Prahl et al.* [1988] and subsequently modified by *Muller et*

Table 3. Cumulative Mass Accumulation Rates of Biomarkers Representing Different Groups of Primary Producers and Zooplankton From RC-27-42[a]

	Σ Diatom, μg cm^{-2} ka^{-1}	Σ Coccolithophorid, μg cm^{-2} ka^{-1}	Σ Dinoflagellate, μg cm^{-2} ka^{-1}	Σ Zooplankton, μg cm^{-2} ka^{-1}	Σ Phytoplankton, μg cm^{-2} ka^{-1}	Σ Sterol, μg cm^{-2} ka^{-1}	Σ Biomarkers, μg cm^{-2} ka^{-1}
Age, ka							
5.0	1.93	1.04	0.63	0.47	3.60	3.03	4.06
7.0	2.17	0.79	0.65	0.77	3.61	3.58	4.38
7.6	5.81	5.03	1.16	1.05	12.00	8.02	13.05
8.3	2.39	1.31	0.67	0.87	4.37	3.93	5.24
10.3	2.48	0.96	0.56	0.55	4.01	3.59	4.56
10.9	4.11	1.39	1.01	1.42	6.51	6.54	7.93
11.6	4.92	1.37	0.93	1.35	7.22	7.20	8.57
13.6	2.99	2.19	0.56	0.52	5.74	4.07	6.26
13.8	1.08	0.92	0.32	0.23	2.32	1.63	2.54
15.2	4.88	3.35	1.66	1.33	9.89	7.87	11.23
16.1	2.42	2.39	0.68	0.64	5.48	3.74	6.12
17.5	1.33	2.06	0.40	0.31	3.79	2.04	4.10
18.1	4.66	4.29	1.25	1.60	10.20	7.52	11.81
18.2	3.29	5.22	1.48	1.82	10.00	6.59	11.82
18.4	3.78	5.51	2.09	1.52	11.38	7.39	12.91
18.4	9.76	8.35	3.20	2.43	21.31	15.39	23.74
18.6	5.55	3.65	2.70	1.66	11.90	9.91	13.56
18.6	8.43	7.95	3.23	2.42	19.61	14.07	22.03
18.7	5.18	6.30	2.56	1.68	14.04	9.42	15.72
18.8	8.24	8.82	3.43	2.60	20.49	14.27	23.09
18.9	4.02	7.74	2.26	1.53	14.02	7.81	15.55
19.0	4.28	5.26	1.95	1.47	11.49	7.70	12.95
19.2	4.13	5.94	1.87	1.54	11.93	7.54	13.48
19.4	5.35	5.54	2.41	2.03	13.29	9.79	15.33
19.5	2.58	3.61	1.12	0.91	7.31	4.61	8.22
19.7	2.24	4.57	0.86	0.93	7.67	4.03	8.60
19.9	2.54	4.80	1.01	0.80	8.35	4.35	9.15
20.0	2.77	2.88	0.40	0.59	6.05	3.76	6.64
21.1	6.46	6.59	2.49	2.05	15.54	11.00	17.58
23.3	4.41	5.17	2.22	1.45	11.80	8.08	13.25
25.5	4.92	6.06	2.35	1.75	13.33	9.03	15.09
27.4	3.29	3.70	1.56	1.12	8.55	5.97	9.67
28.2	3.56	5.04	1.34	1.05	9.94	5.95	10.99
Average Holocene fluxes, μg cm^{-2} ka^{-1}	3.40	1.70	0.80	0.93	5.90	5.13	6.83
Average glacial fluxes, μg cm^{-2} ka^{-1}	4.31	4.92	1.75	1.38	10.98	10.10	12.36
Holocene SD	1.54	1.49	0.23	0.37	3.05	2.05	3.27
Glacial SD	2.11	2.02	0.92	0.65	4.79	3.58	5.42
Holocene RSD%	45.19	87.40	28.64	39.76	51.67	39.98	47.91
Glacial RSD%	48.94	41.10	52.62	46.90	43.67	35.49	43.82

[a]Average fluxes, standard deviations (1σ) and relative standard deviation (RSD) during the glacial (28.1 to 13.6 ka; shaded) and the Holocene (11.6 to 4.5 ka) for each group of biomarkers are also indicated.

al. [1998]. The modification is based on data from new laboratory culture experiments and global core top calibrations:

$$SST(°C) = \left(U_{37}^{K'} - 0.044 \right)/0.033 \qquad (4)$$

[25] Seasonal variations in surface water temperature in the western Arabian Sea are linked to the strength of SW and the NE monsoons during the summer and winter seasons, respectively. There is ample evidence from organic and inorganic geochemical proxies that the SWM was weakened during the glacial period in the western Arabian

Sea [e.g., *Anderson and Prell*, 1993; *Sirocko*, 1991], while average SSTs were relatively lower by about 3°C [*Rostek et al.*, 1997] or 4°C [*Dahl and Oppo*, 2006]. Our average glacial SST estimate (Figure 5d) is about 3°C below the average Holocene SST value, in agreement with previous estimates. There are two main features that stand out from the pattern of SST variability are (1) the significant decrease in temperature prior to the deglacial between 19 and 18 ka B.P. (Figure 5d) and (2) rising postdeglacial SSTs that are punctuated by brief periods of lower SSTs. From 19 to 18 ka B.P., SSTs are maintained between about 21 and 22°C. The lowest SST measured is 15.3°C at 18.5 ka (81 cm depth in the core). Although we have no reason to question the
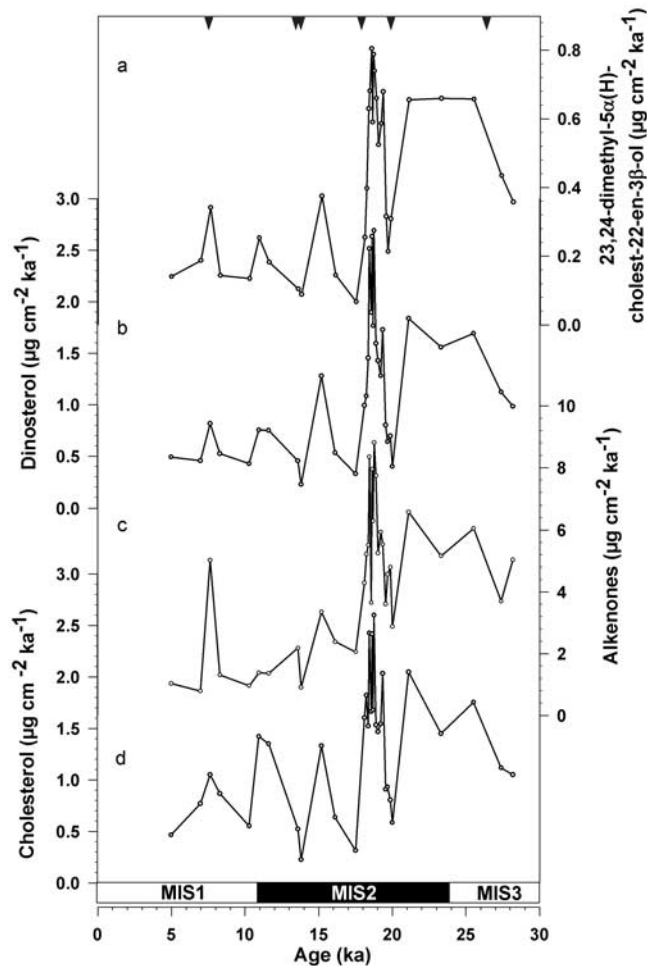
greater temperature variability than other Arabian sea alkenone records, the overall average difference in glacial-Holocene SSTs between our record (3°C) and the others is the same (2°C [*Huguet et al.*, 2006], 3°C [*Rostek et al.*, 1997], and 4°C [*Schulte and Müller*, 2001]). The pattern of variability is dominated by three episodes of lower SSTs in the postdeglacial. Such variability at a single site has been observed in a recent study by *Dahl and Oppo* [2006]. They show convincingly that SSTs can be dramatically different over short temporal and small spatial scales. Indeed, over the entire zone of intense upwelling in the Arabian Sea, *Dahl and Oppo* [2006] show that at 20 ka SSTs were colder compared to modern-day SSTs by anywhere from 1.1 to 4.8°C. At 15 ka, various sites in the upwelling zone recorded SSTs that were 1°C warmer to 1.7°C colder. More importantly, temporal variability in the upwelling zone of
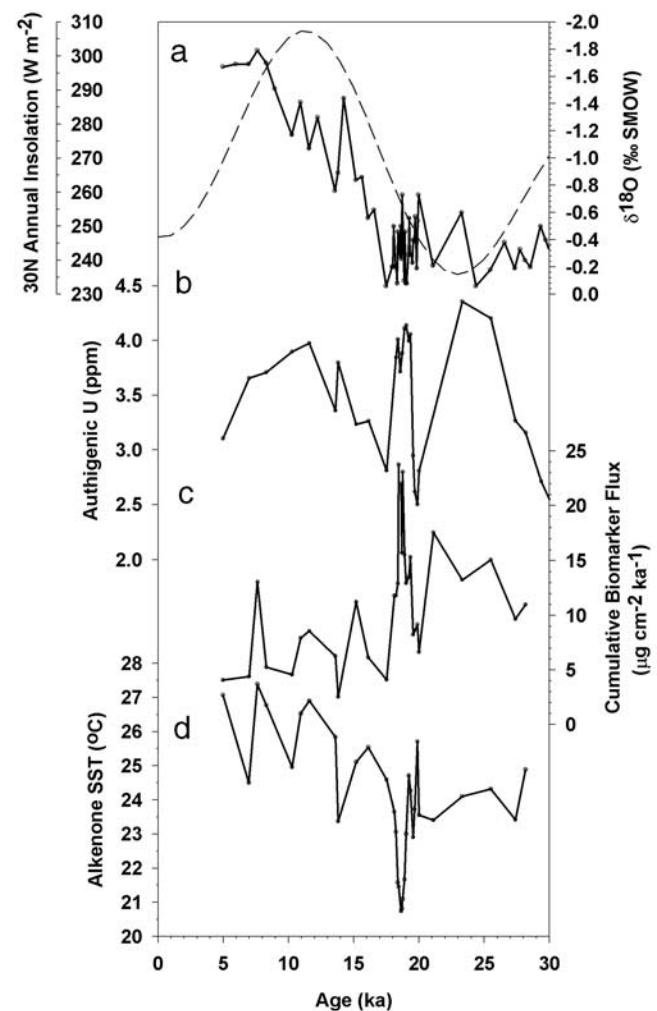

Figure 4. The ^{230}Th-normalized mass accumulation rates of (a) 23,24-dimethyl-5α(H)-cholest-22-en-3β-ol, (b) dinosterol, (c) alkenones ($C_{37:2}$ and $C_{37:3}$ cumulative fluxes), and (d) cholesterol over the last 28 ka. The calibrated radiocarbon dates (triangles at top) and marine isotopic stages (MIS) 1−3 (inset at bottom) are also shown.

validity of the $U_{37}^{K'}$ value measured in this sample, there has been no record of such an extreme SST minimum in the Arabian Sea prior to this study. Unfortunately, the material at this interval in the core has been consumed so that we have not been able to replicate the result.. However, we have attempted to measure alkenones in several nearby samples. Organic extraction and analysis of alkenones for samples within 6 cm of this interval (from 19 to 18.1 ka or 87 to 75 cm) were conducted by two separate analysts on separate dates in order to rule out potential analytical artifacts. Except for the one anomalous data point, the data within the time period of 19 to 18.1 (6 cm on either side of the anomalous point) yield an average value of 21.4°C with a standard deviation of 0.4°C. If we treat the anomalous data point (15.3°C) as an outlier, the observed SSTs are in line with what is observed by others [e.g., *Rostek et al.*, 1997; *Schulte and Müller*, 2001; *Huguet et al.*, 2006; *Dahl and Oppo*, 2006]. Although our alkenone record shows

Figure 5. (a) RC-27-42 oxygen isotope record (solid line) with average annual solar insolation at 30°N (dashed line), (b) authigenic uranium concentrations, (c) cumulative biomarker fluxes representative of diatoms, dinoflagellates, coccolithophorids and zooplankton, and (d) sea surface temperature estimates based on alkenone unsaturation index calibration [*Muller et al.*, 1998] (see text for details) over the last 28 ka.

the Arabian Sea can be similarly large. For example, *Dahl and Oppo* [2006] show that in core 71 KL located only about 60 km from core RC-27-42, estimated SSTs are ~2°C colder at 8 ka than present-day core top SSTs (similar to our variability of 2–3°C in the Holocene). In the same core they show that at 15 ka, estimated SSTs are almost identical to present-day values. Therefore we argue that although the average variability in SSTs in the upwelling zone of the Arabian Sea generally increases from the LGM to the Holocene, higher-frequency variations may also be present that are superimposed on this record.

[26] The average glacial-Holocene change in alkenone-derived paleotemperatures can be compared to temperature estimates based on glacial-Holocene changes in $\delta^{18}O$ once the ice volume effect is removed from the oxygen isotope signal. The lowest (0.06‰) and highest (1.79‰) $\delta^{18}O$ values in sediments from RC-27-42 occur at 7.6 ka and 17.5 ka B.P., respectively. About 1 ± 0.1‰ of the glacial-Holocene range in $\delta^{18}O$ can be explained by global sea level change as a result of changes in continental ice volume [*Schrag et al.*, 2002]. The remaining 0.73‰ is most likely explained by changes in SST and/or sea surface salinity (SSS). An increase in temperature of about 3°C is expected if the 0.73‰ $\delta^{18}O$ depletion that occurred during the last termination is associated with sea surface temperature alone. The agreement between this temperature increase and that determined using the alkenone data may be fortuitous in that the influence of variable sea surface salinity on the oxygen isotope ratios cannot be ruled out. *Sirocko et al.* [1993] dismiss warmer Holocene SSTs as being responsible for the negative shift in their record of *G. ruber* $\delta^{18}O$ from nearby core 74 KL. They reason that intensification of the southwest monsoon during the Holocene is expected to decrease SSTs by inducing cold upwelling in the western Arabian Sea. Our alkenone-derived SSTs, however, provide evidence that intensification of the SWM does not seem to be the controlling factor of western Arabian Sea SSTs during the Holocene, in agreement with the work of *Emeis et al.* [1995] and *Dahl and Oppo* [2006].

[27] Recently, an important problem has been identified in the interpretation of alkenone proxy data. This problem arises because of an inadequate assessment of sediment focusing processes and their effect on apparent SST estimates [*Mollenhauer et al.*, 2003; *Ohkouchi et al.*, 2002]. *Ohkouchi et al.* [2002] reported different ages between fine-grained and coarse-grained components of drift deposits on the Bermuda Rise, while *Mollenhauer et al.* [2003] encountered similar results in sediments from the Benguela upwelling area. Alkenones in the fine-grained fraction consistently yield radiocarbon ages that are 1 to 7 ka older than those of foraminifera in the same interval of sediment. As we have shown, our average ^{230}Th flux to production ratio is close to unity suggesting that sediment redistribution is unlikely to be an issue at our site over the past 28 ka. If there are temporal changes in sediment redistribution, then it is required that these changes in redistribution (i.e., focusing versus winnowing) fortuitously balance each other so that no temporal change in the flux of ^{230}Th occurs over long timescales (i.e., 38 ka), which is an unlikely scenario. Consequently, we suggest that sediment

redistribution has not occurred and that our estimates of SSTs reflect changes in the unsaturation of alkenones produced in the surface mixed water above this site in western Arabian Sea.

4.2. Glacial-Holocene Controls on Primary Production and Sea Surface Paleotemperature

[28] Marine sediments contain organic compounds that have been (1) produced in situ by primary producers and consumers at all trophic levels and/or (2) transported by rivers and dust plumes from their distal sources on land [*Volkman*, 1986]. In recent years, much effort has been focused on identifying lipid biomarker compounds in sediments and the specific source(s) from which they are derived [*Conte et al.*, 1994; *Volkman et al.*, 1998]. Since no single sterol appears to be exclusive to a particular primary producer or animal, it is advised to use multiple markers as indicators of a class of algae or zooplankton [*Dahl et al.*, 2004; *Wakeham et al.*, 2002].

[29] One of the main concerns in employing biomarkers as paleoproxies for primary production and phytoplankton community structure is differential preservation of organic compounds in the sedimentary record (see review by *Meyers* [2003, and references therein]). Some biomarkers appear to be less resistant to degradation than others and this can pose complications in interpreting the biomarker record. The influence of preferential preservation of organic matter becomes more pertinent if bottom water oxygenation is variable and anoxia is not consistently maintained across the sediment-water interface. The site of our core lies below today's depth of the oxygen minimum zone, so it is unlikely that variable oxic/anoxic conditions at this site have existed in the past. Preferential preservation and postdepositional exposure of biomarkers to oxygenated waters do not seem to have played a major role in sediments from RC-27-42. If preferential degradation were an issue, one would expect accumulation rates of sterols, which are more labile than refractory alkenones, to decrease with depth [*Dahl et al.*, 2004; *Werne et al.*, 2000]. We observe the opposite trend in sediments from the western Arabian Sea, i.e., higher fluxes of sterols are observed in deeper sediments. Indeed, the average cumulative flux of sterols (Table 3) during the glacial is roughly double (10.1 μg cm^{-2} ka^{-1}) that during the Holocene (5.1 μg cm^{-2} ka^{-1}). In addition, the highest cumulative biomarker fluxes (CBF) occur in the deeper sections of the core compared with the shallower depths (Figure 5c). One might ascribe higher CBFs in the glacial as a consequence of higher glacial MARs and enhanced preservation. Although average MARs are about 35% higher, on average, in the glacial compared to those in the Holocene, over the same time period, CBF fluxes are higher by ~55%. Another piece of evidence that suggests biomarker fluxes have not been influenced by diagenesis is that these fluxes are coincident with the highest authigenic uranium concentrations, a proxy for the export of total organic carbon (TOC) to the sediments [e.g., *Pourmand et al.*, 2004; *McManus et al.*, 2005]. Authigenic uranium concentrations range from about 2.5 to 4.4 ppm (Figure 5b). Average authigenic U concentrations remain constant throughout the Holocene and glacial (~3.5 ppm), although

their patterns of variability differ during the two time periods. Hence we believe that the observed pattern organic biomarker MARs through time is representative of a changing distribution of primary producers and consumers in the water column, and not an artifact of postdepositional diagenetic processes.

[30] Enhanced primary productivity in the Arabian Sea is closely tied to upwelling of cold nutrient-rich waters in the western and NE Arabian Sea during the SWM and convective mixing of surface waters in the eastern and central Arabian Sea [*Rixen et al.*, 1996] during the NEM. On the basis of CBFs, we suggest that primary production was high throughout the glacial period with maximum production occurring at exactly the time when the lowest SSTs occur between 19 and 18.1 ka B.P. (Figures 5b–5d). We interpret colder SSTs during the glacial period as an indicator for strengthened NEM winds and/or an increase in the seasonal duration of the NEM. During times of intensified NEM winds, cold air blows from the snow covered areas of the Himalayas and the Tibetan Plateau lowering SSTs across the Arabian Sea. The pulse of lowest SSTs between 19 and 18.1 ka B.P. lags by 4.5 ka the minimum in annual insolation at 30°N (Figure 5a). We propose that low glacial SSTs during the glacial are due to the dominating influence of a strong NEM that resulted in deep winter convective mixing. *Reichart et al.* [1998] interpreted the presence of *G. truncatulinoides* and/or *G. crassaformis* in the northern Arabian Sea as indicators for a period of deep convective mixing (to depths as low as 800 m below the sea surface) induced by an intensified NEM. While *Reichart et al.* [1998] associate the timing of this cold interval in SSTs with North Atlantic (NA) Heinrich event 1 (HE1), in our record the interval of lowest SSTs coincides with maxima in primary production and clearly precedes the NA HE1 at 16.8 ka (S. Hemming, personal communication, 2006). Moreover, SSTs increase rapidly to values higher than 25°C at 16.8 ka. The timing of this increase in SST, which is synchronous with the abrupt drop in CBFs, appears to be coincident with the timing of HE 1 in the North Atlantic.

[31] A possible link between NA climate and low-latitude, high-frequency variability during the glacial period has been proposed by *Fang et al.* [1999]. They suggest that the strength of the Asian summer and winter monsoons is in part controlled by a "swing" in the position of the midlatitude westerlies. During times of high insolation the westerlies are shifted north of the Tibetan Plateau, thereby establishing a low-pressure system and causing an intensified Asian summer monsoon. In contrast, when insolation is relatively low, westerlies are shifted southward over the Tibetan Plateau, and induce intensified winter monsoon winds. According to this model, the position of the westerlies is also influenced by abrupt (higher frequency than orbital) expansions of polar air. Such abrupt cold events that are associated with shifting westerlies could explain therefore intensified NE monsoon winds, deep convective oceanic mixing accompanied by elevated primary productivity and low SSTs observed between 19 and 18.1 ka at our site. This N-S shift in Northern Hemisphere westerlies, which, in turn, is related to SW versus NE monsoon dominance in the Arabian Sea, may coincide with movement of the ITCZ due

to changing intensities of the trade winds on abrupt climate change timescales [e.g., *Ivanochko et al.*, 2005].

[32] Low SSTs and high CBFs generally prevail during the glacial period (Figures 5c–5d). This is not unexpected because of the relationship between NE monsoon wind intensity and mixing of cold nutrient-rich waters that are otherwise trapped below the thermocline. Interestingly this pattern reverses during the deglacial (which begins at about 17 ka) and during the Holocene with peaks of high CBFs coinciding with peaks of high SSTs. In the modern-day Arabian Sea, advection of nutrients during the summer SWM results in high primary production in regions of relatively higher SSTs located farther offshore from the zone of upwelling closest to the Oman Margin [*Honjo et al.*, 1999; *Wakeham et al.*, 2002]. Hence the coincidence between the high SSTs and CBFs during this interval may be related to distance of our site from the margin where the most intense upwelling occurs.

4.3. Glacial-Holocene Planktonic Community Structure Variability

[33] Organic biomarker proxies more accurately represent the planktonic ecosystem compared to the inorganic proxies of silica and carbonate because organisms differ in rates of production of opal or carbonate tests, dissolution can influence the preservation of tests, and some organisms do not produce tests or hard parts. In such cases, relative abundance of organic biomarkers associated with different classes of primary producers and consumers can be successfully employed to interpret changes in planktonic community structure on glacial-interglacial timescales [e.g., *Werne et al.*, 2000]. Assuming minimal differences in postdepositional preservation between class-specific biomarkers associated with these phytoplankton, it seems that the relative contribution of dinoflagellates to primary production in the western Arabian Sea has not changed markedly during the transition from glacial to Holocene, or within either time period (Figure 6a). A similar observation was made by *Schubert et al.* [1998] in the eastern Arabian Sea for an extended period of 200 ka.

[34] In contrast, the fluxes of cumulative diatom and coccolithophorid biomarkers relative to the total cumulative biomarker fluxes as a function of time show climate-related changes during the last 28 ka (Figure 6a). The contribution of diatom biomarkers to primary production increases relative to the contribution of coccolithophorid biomarkers upon the transition at 17 ka from the glacial to the deglacial. This relationship is better illustrated when the ratio of the fluxes of these two classes of primary producers in the Arabian Sea are plotted through time (Figure 6b). Nutrient availability (particularly silica) is one of the most important limiting factors in the distribution of diatoms in the Arabian Sea [*Wakeham et al.*, 2002]. Diatoms are known to be the most dominant primary producers in cold-upwelling waters with a high availability of silica. Coccolithophorids, on the other hand, compete better in waters of low nutrient availability [*Honjo et al.*, 1999; *Ramaswamy and Gaye*, 2006]. Following the transition from glacial to deglacial time, SWM intensification and upwelling of silica-rich waters along the Oman margin may have contributed to

Figure 6. (a) Fluxes of major groups of organic biomarkers relative to the cumulative biomarker flux. The relative fluxes have been determined by placing individual biomarker compounds into one of the 4 planktonic groups, summing the fluxes of biomarker compounds within each group, and then taking the ratio of sum of one group of organism fluxes to the sum of the entire cumulative group of organism fluxes. (b) Ratio of diatom to coccolithophorid flux plotted against sediment age. The relative flux of diatoms increases beginning at about 17 ka. Marine isotopic stages (MIS) 1–3 are shown in inset at the bottom of the graph.

the higher abundance of diatoms relative to coccolithophorids. Indeed, an analogy exists in the modern-day planktonic seasonal systematics of the Arabian Sea. Studies of water column sediment traps from the western Arabian Sea show that the ratio of the relative flux of diatoms to coccolithophorids is higher during the summer SWM than that during the winter NEM [*Wakeham et al.*, 2002; *Ramaswamy and Gaye*, 2006]. Hence, on the basis of modern observations of the temporal distribution of diatom and coccolithophorid blooms during the NE and SW monsoons, we suggest that coccolithophorids dominate during the glacial period when the NEM winds play a major role, and diatoms are increased relative to coccolithophorids during the deglacial and Holocene when the SWM is stronger.

[35] The fact that both the fluxes of planktonic organisms and eolian material are responding to climate variability may have implications for our understanding of feedback processes which affect the biogeochemical cycle of carbon. One possible mechanism through which atmospheric CO_2 content may have been regulated on glacial to interglacial timescales is the efficiency of the biological pump as a result of iron fertilization [*Martin*, 1990]. We do not observe any relationship between the high-frequency pattern of variability of the cumulative or individual biomarker flux (proxy for productivity) and eolian flux (the only source of Fe to our site, Figure 2c). However, both the average cumulative flux of biomarkers representing all planktonic groups and eolian flux are higher during the last glacial period than both fluxes during the Holocene. These contrasting results make it difficult to draw any conclusions about the importance of oceanic Fe fertilization on atmospheric CO_2 contents.

[36] While bulk organic matter proxies do not distinguish between the source(s) of organic matter, biomarkers allow greater insight into the relationship between organisms at different trophic levels and their control on the planktonic community structure within the sedimentary record. If we examine controls on phytoplankton biomass from the top-down perspective, we find that accumulation rates for cholesterol, a useful proxy for zooplankton and other invertebrates, show a significant statistical correlation with phytoplankton accumulation rates (r^2 at 95% confidence = 0.85). This suggests that secondary production is linked with phytoplankton biomass over the last 28 ka in the western Arabian Sea. Specifically, accumulation rates of cholesterol are highly correlated with groups of biomarkers that represent dinoflagellates (r^2 at 95% confidence = 0.85), diatoms (r^2 at 95% confidence = 0.79) and coccolithophorids (r^2 at 95% confidence = 0.66). Cholesterol is produced by numerous zooplankton or even other marine fauna [*Volkman*, 1986], so we do need to be cautious about the connections we make between zooplankton and specific phytoplankton accumulation rates. Nevertheless, the relative abundance of zooplankton does not appear to have undergone significant changes from glacial to interglacial periods, which suggests that controls on the ratio of diatom to coccolithophorids may be related to grazing processes (or trophic top-down processes) in the Arabian Sea basin. Alternatively, cholesterol may be derived from the phytoplankton community, in which case our results support

controls on phytoplankton biomass via bottom-up processes (i.e., availability of nutrients) in the Arabian Sea during the last 30 ka.

[37] Even though our data do not allow us to determine the extent to which predation has exerted control on the zooplankton biomass (and hence the flux of cholesterol), the possibility of higher trophic levels on zooplankton biomass cannot be ignored in interpreting the biomarker data.

5. Summary

[38] The ^{230}Th-normalized fluxes of organic biomarkers for major primary producers (diatoms, coccolithophorids and dinoflagellates) and zooplankton, along with alkenone-derived SSTs, have been measured in a 28-ka record from core RC-27-42 in the western Arabian Sea. We interpret our biomarker and inorganic proxy data in the context of changes in the intensity of the intensity of SWM versus NEM wind strength on glacial-interglacial and abrupt climate timescales. Primary production and sea surface temperature appear to have been under the influence of a stronger NEM wind system between 28 and 17 ka. Average phytoplankton biomass is higher during glacial times than during the Holocene, while glacial average SSTs are 3°C lower than average Holocene SSTs. The coldest SSTs induce deep convective mixing, which increases the availability of nutrients in the euphotic zone. As a result the highest levels of phytoplankton biomass are associated with the lower SSTs. A possible cause for this interval of low SST and high productivity between 19 and 18.1 ka B.P. may be a southward shift in the position of the westerlies. Following 17 ka and continuing into the Holocene, SSTs increase to relatively higher values, primarily as a consequence of higher insolation at this latitude and associated weakening of NEM winds. The relationship between SST and phytoplankton biomass also changes during the Holocene, with high cumulative accumulation rates of organic biomarkers occurring at times of high SSTs.

[39] A comparison between the relative flux of organic biomarkers representing four major groups of primary producers and consumers also enable us to track changes in planktonic community structure from the glacial to the Holocene. Whereas the fluxes of dinoflagellate biomarkers relative to the total flux of biomarkers remain nearly constant for the last 28 ka, higher relative abundances of silicate/calcite-producing phytoplankton in our site during the Holocene compared with the glacial period are opposite of what is expected if glacial atmospheric CO_2 levels are to be explained by higher abundance of silicate-producing organisms. We attribute this shift in relative abundance of diatoms and coccolithophorids to higher availability of silica during the Holocene. The relative abundance of zooplankton (cholesterol) shows little variability, which indicates that bottom-up processes may have remained dominant in controlling the distribution of planktonic organisms at the trophic levels of this site during the last 28 ka.

References

Altabet, M. A., M. J. Higginson, and D. W. Murray (2002), The effect of millennial-scale changes in Arabian Sea denitrification on atmospheric CO_2, *Nature*, *415*(6868), 159–162.

Anderson, D. M., and W. L. Prell (1993), A 300 kyr record of upwelling off Oman during the late Quaternary: Evidence of the Asian southwest monsoon, *Paleoceanography*, *8*(2), 193–208.

Banakar, V. K., et al. (2005), Monsoon related changes in sea surface productivity and water column denitrification in the eastern Arabian Sea during the last glacial cycle, *Mar. Geol.*, *219*(2–3), 99–108.

Bhushan, R., S. Chakraborty, and S. Krishnaswami (1994), Physical research laboratory (chemistry) radiocarbon date list, *Radiocarbon*, *36*(2), 251–256.

Brassell, S. C., M. Sarnthein, G. Eglinton, I. T. Marlowe, and U. Pflaumann (1986), Molecular stratigraphy: A new tool for climatic assessment, *Nature*, *320*(6058), 129–133.

Brock, J. C., and C. R. McClain (1992), Interannual variability in phytoplankton blooms observed in the northwestern Arabian Sea during the southwest monsoon, *J. Geophys. Res.*, *97*(C1), 733–750.

Budziak, D., et al. (2000), Late Quaternary insolation forcing on total organic carbon and C_{37} alkenone variations in the Arabian Sea, *Paleoceanography*, *15*(3), 307–321.

Canuel, E. A., and C. S. Martens (1993), Seasonal variations in the sources and alteration of organic matter associated with recently-deposited sediments, *Org. Geochem.*, *20*(5), 563–577.

Chavez, F. P., and J. R. Toggweiler (1995), Physical estimates of global new production: The upwelling contribution, in *Upwelling in the Ocean: Modern Processes and Ancient Records*, edited by C. P. Summerhayes et al., pp. 313–320, John Wiley, New York.

Clemens, S. C., and W. L. Prell (1990), Late Pleistocene variability of Arabian Sea summer monsoon winds and continental aridity: Eolian records from the lithogenic component of deep-sea sediments, *Paleoceanography*, *5*(2), 109–145.

Clemens, S., G. Weedon, W. Prell, D. Murray, and G. Shimmield (1991), Forcing mechanisms of the Indian Ocean monsoon, *Nature*, *353*(6346), 720–725.

Conte, M. H., J. K. Volkman, and G. Eglinton (1994), Lipid biomarker of the Haptophyta, in *The Haptophyte Algae*, edited by J. C. Green and B. S. C. Leadbeater, pp. 351–377, Clarendon, Oxford, U.K.

Dahl, K. A., and D. W. Oppo (2006), Sea surface temperature pattern reconstructions in the Arabian Sea, *Paleoceanography*, *21*, PA1014, doi:10.1029/2005PA001162.

Dahl, K. A., D. J. Repeta, and R. Goericke (2004), Reconstructing the phytoplankton community of the Cariaco Basin during the Younger Dryas cold event using chlorin steryl esters, *Paleoceanography*, *19*, PA1006, doi:10.1029/2003PA000907.

Dutta, K., R. Bhushan, and B. L. K. Somayajulu (2001), ΔR correction values for the northern Indian Ocean, *Radiocarbon*, *43*(2A), 483–488.

Emeis, K. C., D. Schulz-Bull, D. M. Anderson, H. Doose, and D. Kroon (1995), Sea-surface temperatures and the history of monsoon upwelling in the northwest Arabian Sea during the last 500,000 years, *Quat. Res.*, *43*(3), 355–361.

Fang, X. M., et al. (1999), Asian summer monsoon instability during the past 60,000 years: Magnetic susceptibility and pedogenic evidence from the western Chinese Loess Plateau, *Earth Planet. Sci. Lett.*, *168*(3–4), 219–232.

Findlater, J. (1974), The low-level cross-equatorial jet stream of the western Indian Ocean, *Weather*, *29*, 411–416.

Francois, R., M. Frank, M. M. Rutgers van der Loeff, and M. P. Bacon (2004), ^{230}Th normalization: An essential tool for interpreting sedimentary fluxes during the late Quaternary,

Paleoceanography, *19*, PA1018, doi:10.1029/2003PA000939.

Haake, B., et al. (1993), Seasonality and inter-annual variability of particle fluxes to the deep Arabian Sea, *Deep Sea Res., Part I*, *40*(7), 1323–1344.

Hales, B., T. Takahashi, and L. Bandstra (2005), Atmospheric CO_2 uptake by a coastal upwelling system, *Global Biogeochem. Cycles*, *19*, GB1009, doi:10.1029/2004GB002295.

Henderson, G. M., and R. F. Anderson (2003), The U-series toolbox for paleoceanography, in *U-Series Geochemistry, Rev. Mineral. Geochem.* vol. 52, edited by B. Bourdon et al., pp. 493–531, Mineral. Soc. of Am., Washington, D. C.

Henderson, G. M., A. M. E. Winguth, C. Heinze, and R. F. Anderson (1999), Global distribution of the ^{230}Th flux to ocean sediments constrained by GCM modeling, *Deep Sea Res., Part I*, *46*(11), 1861–1893.

Herbert, T. D., J. D. Schuffert, D. Thomas, C. Lange, A. Weinheimer, A. Peleo-Alampay, and J.-C. Herguera (1998), Depth and seasonality of alkenone production along the California margin inferred from a core top transect, *Paleoceanography*, *13*(3), 263–271.

Higginson, M. J., M. A. Altabet, L. Wincze, T. D. Herbert, and D. W. Murray (2004), A solar (irradiance) trigger for millennial-scale abrupt changes in the southwest monsoon?, *Paleoceanography*, *19*, PA3015, doi:10.1029/2004PA001031.

Honjo, S., V. Ittekkot, J. Dymond, and W. Prell (1999), Monsoon-controlled export fluxes to the interior of the Arabian Sea, *Deep Sea Res., Part II*, *46*(8–9), 1859–1902.

Huguet, C., J.-H. Kim, J. S. Sinninghe Damsté, and S. Schouten (2006), Reconstruction of sea surface temperature variations in the Arabian Sea over the last 23 kyr using organic proxies (TEX_{86} and $U^{K'}_{37}$), *Paleoceanography*, *21*, PA3003, doi:10.1029/2005PA001215.

Ivanochko, T. S., et al. (2005), Variations in tropical convection as an amplifier of global climate change at the millennial scale, *Earth Planet. Sci. Lett.*, *235*(1–2), 302–314.

Marcantonio, F., et al. (2001), Abrupt intensification of the SW Indian Ocean monsoon during the last deglaciation: Constraints from Th, Pa, and He isotopes, *Earth Planet. Sci. Lett.*, *184*(2), 505–514.

Martin, J. H. (1990), Glacial-interglacial CO_2 change: The iron hypothesis, *Paleoceanography*, *5*(1), 1–13.

Martinson, D. G., et al. (1987), Age dating and the orbital theory of the ice ages: Development of a high-resolution 0 to 300,000–year chronostratigraphy, *Quat. Res.*, *27*(1), 1–29.

McGee, D., F. Marcantonio, and J. Lynch-Stieglitz (2007), Deglacial changes in dust flux in the eastern equatorial Pacific, *Earth Planet. Sci. Lett.*, *257*(1–2), 215–230, doi:10.1016/j.epsl.2007.02.033.

McManus, J., W. M. Berelson, G. P. Klinkhammer, D. E. Hammond, and C. Holm (2005), Authigenic uranium: Relationship to oxygen penetration depth and organic carbon rain, *Geochim. Cosmochim. Acta*, *69*, 95–108.

Meyers, P. A. (2003), Applications of organic geochemistry to paleolimnological reconstructions: A summary of examples from the Laurentian Great Lakes, *Org. Geochem.*, *34*(2), 261–289.

Mollenhauer, G., et al. (2003), Asynchronous alkenone and foraminifera records from the Benguela Upwelling System, *Geochim. Cosmochim. Acta*, *67*(12), 2157–2171.

Muller, P. J., I. Von Storch, A. Rosell-Mele, G. Kirst, and G. Ruhland (1998), Calibration of the alkenone paleotemperature index $U^{K'}_{37}$ based core-tops from the eastern South Atlantic and the global ocean (60°N–60°S), *Geochim. Cosmochim. Acta*, *62*(10), 1757–1772.

Naidu, P. D. (1998), Driving forces of Indian summer monsoon on Milankovitch and sub-Milankovitch time scales: A review, *J. Geol. Soc. India*, *52*(3), 257–272.

Naidu, P. D., and B. A. Malmgren (2005), Seasonal sea surface temperature contrast between the Holocene and last glacial period in the western Arabian Sea (Ocean Drilling Project Site 723A): Modulated by monsoon upwelling, *Paleoceanography*, *20*, PA1004, doi:10.1029/2004PA001078.

Nair, R. R., V. Ittekkot, S. J. Manganini, V. Ramaswamy, B. Haake, E. T. Degens, B. N. Desai, and S. Honjo (1989), Increased particle flux to the deep ocean related to monsoons, *Nature*, *338*(6218), 749–751.

Ohkouchi, N., T. I. Eglinton, L. D. Keigwin, and J. M. Hayes (2002), Spatial and temporal offsets between proxy records in a sediment drift, *Science*, *298*(5596), 1224–1227.

Paillard, D., L. Labeyrie, and P. Yiou (1996), Macintosh program performs time series analysis, *Eos Trans. AGU*, *77*, 379.

Pourmand, A., F. Marcantonio, and H. Schulz (2004), Variations in productivity and eolian fluxes in the northeastern Arabian Sea during the past 110 ka, *Earth Planet. Sci. Lett.*, *221*(1–4), 39–54.

Pourmand, A., F. Marcantonio, T. S. Bianchi, E. A. Canuel, and E. J. Waterson (2005), Radionuclide and biomarker proxies of past ocean circulation and productivity in the Arabian Sea, *Geophys. Res. Lett.*, *32*, L10610, doi:10.1029/2005GL022612.

Prahl, F. G., and S. G. Wakeham (1987), Calibration of unsaturation patterns in long-chain ketone compositions for palaeotemperature assessment, *Nature*, *330*(6146), 367–369.

Prahl, F. G., L. A. Muehlhausen, and D. L. Zahnle (1988), Further evaluation of long-chain alkenones as indicators of paleoceanographic conditions, *Geochim. Cosmochim. Acta*, *52*(9), 2303–2310.

Prahl, F. G., G. L. Cowie, G. J. De Lange, and M. A. Sparrow (2003), Selective organic matter preservation in "burn-down" turbidites on the Madeira Abyssal Plain, *Paleoceanography*, *18*(2), 1052, doi:10.1029/2002PA000853.

Ramaswamy, V., and B. Gaye (2006), Regional variations in the fluxes of foraminifera carbonate, coccolithophorid carbonate and biogenic opal in the northern Indian Ocean, *Deep Sea Res., Part I*, *53*(2), 271–293.

Reichart, G. J., L. J. Lourens, and W. J. Zachariasse (1998), Temporal variability in the northern Arabian Sea oxygen minimum zone (OMZ) during the last 225,000 years, *Paleoceanography*, *13*(6), 607–621.

Rixen, T., B. Haake, V. Ittekkot, M. V. S. Guptha, R. R. Nair, and P. Schlüssel (1996), Coupling between SW monsoon-related surface and deep ocean processes as discerned from continuous particle flux measurements and correlated satellite data, *J. Geophys. Res.*, *101*(C12), 28,569–28,582.

Rixen, T., M. V. S. Guptha, and V. Ittekkot (2005), Deep ocean fluxes and their link to surface ocean processes and the biological pump, *Prog. Oceanogr.*, *65*(2–4), 240–259.

Rogalla, U., and H. Andruleit (2005), Precessional forcing of coccolithophore assemblages in the northern Arabian Sea: Implications for monsoonal dynamics during the last 200,000 years, *Mar. Geol.*, *217*(1–2), 31–48.

Rostek, F., C. Sonzogni, G. Ganssen, E. Bard, and L. Beaufort (1997), Sea surface temperature and productivity records for the last 240 kyr on the Arabian Sea, *Deep Sea Res., Part II*, *44*(6–7), 1461–1480.

Rowland, S. J., and J. K. Volkman (1982), Biogenic and pollutant alphatic hydrocarbons in *Mytilus edulis* from the North Sea (*Emiliania huxleyi*), *Mar. Environ. Res.*, *7*(2), 117–130.

Schrag, D. P., et al. (2002), The oxygen isotopic composition of seawater during the Last Glacial Maximum, *Quat. Sci. Rev.*, *21*(1–3), 331–342.

Schubert, C. J., et al. (1998), Stable phytoplankton community structure in the Arabian sea over the past 200,000 years, *Nature*, *394*(6693), 563–566.

Schulte, S., and P. Müller (2001), Variations of sea surface temperature and primary productivity during Heinrich and Dansgaard-Oeschger events in the northeastern Arabian Sea, *Geo Mar. Lett.*, *21*(3), 168–175.

Schulte, S., J. Rullkotter, O. Marchal, F. Rostek, and E. Bard (1999), Variations of oxygen-minimum and primary productivity recorded in sediments of the Arabian Sea, *Earth Planet. Sci. Lett.*, *173*(3), 205–221.

Schulz, H., U. von Rad, and H. Erlenkeuser (1998), Correlation between Arabian Sea and Greenland climate oscillations of the past 110,000 years, *Nature*, *393*(6680), 54–57.

Sirocko, F. (1991), Deep-sea sediments of the Arabian Sea: A paleoclimatic record of the southwest-Asian summer monsoon, *Geol. Rundsch.*, *80*(3), 557–566.

Sirocko, F., and H. Lange (1991), Clay-mineral accumulation rates in the Arabian Sea during the late Quaternary, *Mar. Geol.*, *97*(1–2), 105–119.

Sirocko, F., et al. (1993), Century-scale events in monsoonal climate over the past 24,000 years, *Nature*, *364*(6435), 322–324.

Sirocko, F., D. Garbe-Schonberg, and C. Devey (2000), Processes controlling trace element geochemistry of Arabian Sea sediments during the last 25,000 years, *Global Planet. Change*, *26*(1–3), 217–303.

Southon, J., W. W. S. Yim, M. Kashgarian, M. Fontugne, and B. Metivier (2002), Marine reservoir corrections for the Indian Ocean and Southeast Asia, *Radiocarbon*, *44*(1), 167–180.

Stuiver, M., and P. J. Reimer (1993), Extended ^{14}C data base and revised CALIB 3.0 ^{14}C age calibration program, *Radiocarbon*, *35*(1), 215–230.

Tamburini, F., K. B. Föllmi, T. Adatte, S. M. Bernasconi, and P. Steinmann (2003), Sedimentary phosphorus record from the Oman margin: New evidence of high productivity during glacial periods, *Paleoceanography*, *18*(1), 1015, doi:10.1029/2000PA000616.

Taylor, S. R., and S. M. McLennan (1985), *The Continental Crust: Its Composition and Evolution*, Blackwell Sci., Malden, Mass.

Volkman, J. K. (1986), A review of sterol markers for marine and terrigenous organic matter, *Org. Geochem.*, *9*(2), 83–99.

Volkman, J. K., et al. (1998), Microalgal biomarkers: A review of recent research developments, *Org. Geochem.*, *29*(5–7), 1163–1179.

Wakeham, S. G., C. Lee, M. L. Peterson, and J. I. Hedges (2002), Lipid biomarker fluxes in the Arabian Sea, with a comparison to the equa-

torial Pacific Ocean, *Deep Sea Res., Part II*, *49*(12), 2265–2301.

Werne, J. P. H., D. J. Hollander, T. W. Lyons, and L. C. Peterson (2000), Climate-induced variations in productivity and planktonic ecosystem structure from the Younger Dryas to Holocene in the Cariaco Basin, Venezuela, *Paleoceanography*, *15*(1), 19–29.

———————————

T. S. Bianchi, Department of Oceanography, Texas A&M University, Room 403AB, College Station, TX 77843-3146, USA.

E. A. Canuel and E. J. Waterson, Virginia Institute of Marine Science, Chespeake Bay Hall, Gloucester Point, VA 23062, USA.

F. Marcantonio, Department of Geology and Geophysics, Texas A&M University, Room 305, M. T. Halbouty Building, College Station, TX 77843, USA. (marcantonio@geo.tamu.edu)

A. Pourmand, Chicago Center for Cosmochemistry, Department of Geophysical Sciences, University of Chicago, 5734 South Ellis Avenue, Chicago, IL 60637, USA.